Microwave frequency comb Doppler reflectometer applying fast digital data acquisition system in LHD

journal or publication title	Review of Scientific Instruments
volume	89
number	10
page range	10H118
year	2018-10
URL	http://doi.org/10.15047/00012484

doi: 10.1063/1.5035118

This manuscript was accepted by Rev. Sci.Instrum. Click here to see the version of record.

Microwave frequency comb Doppler reflectometer applying fast digital data acquisition system in LHD[a)]

T. Tokuzawa,[1] H. Tsuchiya,[1] T. Tsujimura,[1] M. Emoto,[1] H. Nakanishi,[1] S. Inagaki,[2] K. Ida,[1,3] H. Yamada,[1,3] A. Ejiri,[4] K. Y. Watanabe,[1,5] K. Oguri,[5] T. Akiyama,[1] K. Tanaka,[1] I. Yamada,[1] and LHD Experiment Group [1,c)]

[1]*National Institutes of Natural Sciences, National Institute for Fusion Science, Toki 509-5292, Japan*
[2]*Research Institute for Applied Mechanics, Kyushu University, Kasuga 816-8580, Japan*
[3]*SOKENDAI (The Graduate University for Advanced Study), 322-6 Oroshi, Toki-city, 509-5292, Japan*
[4]*Graduate School of Frontier Sciences, The University of Tokyo, Kashiwa 277-8561, Japan*
[5]*Department of Energy Engineering and Science, Nagoya University, Furo-cho, Chikusa-ku, Nagoya, 464-8601*

(Presented XXXXX; received XXXXX; accepted XXXXX; published online XXXXX)
(Dates appearing here are provided by the Editorial Office)

We succeeded in increasing the radial observation points of microwave frequency comb Doppler reflectometer system from 8 to 20 (or especially up to 45) using the high sampling rate of 40 GS/s digital signal processing. For a new acquisition system, the estimation scheme of the Doppler shifted frequency is constructed and compared with the conventional technique. Also, the fine radial profile of perpendicular velocity is obtained, and it is found that the perpendicular velocity profile is consistent with the $E \times B$ drift velocity one.

I. INTRODUCTION

Regarding the study of the behavior of the turbulence affecting transport, the multi-scale interaction of turbulence between macro-, meso-, and micro-scale structures is receiving much attention at present. For this aim, higher spatial and temporal resolution diagnostics have been developed and applied in several devices[1]. Microwave Doppler reflectometry (also called Doppler back-scattering: DBS) has the capability to measure the perpendicular velocity $v_\perp$ of electron density fluctuations, the radial electric field E_r, and the perpendicular wavenumber spectrum $S(k_\perp)$ in magnetized confinement plasmas, using its unique advantage that is the combination with the back-scattering method (which provides a wavenumber resolution) and reflectometry (which provides a high-spatial resolution)[2]. As a result, a number of systems have been used in worldwide fusion plasma devices, such as tokamaks (Tuman-3M[3], ASDEX Upgrade[4-6], Tore Supra[7,8], DIII-D[9,10], JT-60U[11], MAST[12], and JET[13]) and helical/stellarators (Wendelstein 7-AS[2,14], TJ-II[15], and LHD[16,17]).

The principle of Doppler reflectometry is explained simply as follows. When a probing microwave beam is injected into a plasma and approaches a cutoff layer with an oblique angle to the cutoff surface, a backscattering occurs caused by the density fluctuations which matches the Bragg condition, i.e., $k = -2k_i$ (where k_i is the local wave vector of the probing beam). For the example in the Large Helical Device (LHD)[18], the range of the fluctuation wavenumber of around 2 – 15 cm^{-1} is designed to correspond to the ion temperature gradient (ITG) mode

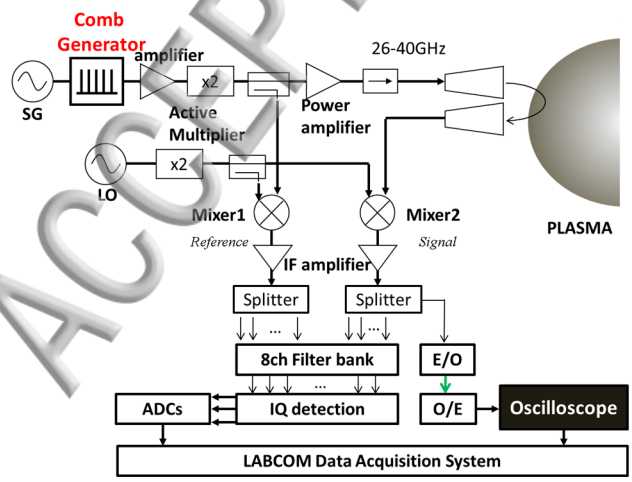

FIG. 1. (Color online). Schematic of the Ka-band microwave circuit for the Doppler reflectometer comprising a comb generator. A synthesized signal generator (SG) is used as a modulator. A 30 dB amplifier and an active multiplier provide the ka-band probe wave. A local oscillator (LO) is used for heterodyne detection. Two intermediate frequency (IF) components, which are indicated as "*Reference*" and "*Signal*," are generated in each Mixer. Each IF signal is divided in the splitter. The filter bank system comprises eight band pass filters for quadrature signal detection. The output of IQ detection is fed to the 1 MHz/10 MHz data acquisition system (ADC). Also, a portion of the splitter output is fed to an electro-optical converter set (E/O and O/E) and transmitted via an optical fiber directly to the diagnostic room for direct signal acquisition of the wideband oscilloscope. The LABCOM data acquisition system collects the all of the acquired signal on the real-time and also controls the acquisition setting via the web site.

[a)]Published as part of the Proceedings of the 22nd Topical Conference on High-Temperature Plasma Diagnostics (HTPD 2018) in San Diego, California, USA.
[b)]Author to whom correspondence: tokuzawa@nifs.ac.jp
[c)]Y. Takeiri *et al*., Nucl. Fusion **57**, 102923 (2017) .

as for the trapped electron mode (TEM) turbulence[19, 20]. The detected power of the backscattered radiation is proportional to the density fluctuation amplitude and the scattered signal frequency is Doppler shifted by the propagation velocity of the density fluctuations. The Doppler shift is given by $\omega_D = v \cdot k \approx v_\perp k_\perp = k_\perp (v_{E\times B} + v_{ph})$, where $v_{E\times B}$ is a composition of the plasma background $E \times B$ drift velocity and v_{ph} is the intrinsic phase velocity of the density fluctuations. If v_{ph} is known or $v_{ph} << v_{E\times B}$ (which is usually satisfied at the plasma edge in magnetically confined devices and shown later in the LHD's results), the radial electric field E_r can be extracted from the measurement of the perpendicular velocity through $E_r = v_\perp B$, where B is the absolute local value of the magnetic field.

In LHD, a multi frequency channel Doppler reflectometer system has been developed[17]. The system, which uses a frequency comb generator as a source and is constructed using a filter bank IQ detection for the Doppler shifted frequency calculation, is utilized for measuring not only the spatial structure of the parameters, but also the temporal relationship between two (or many) points in space. These measurements are quite helpful for evaluating plasma turbulence, transport, and confinement phenomena. Recently, the fast digital data acquisition system including a high sampling rate oscilloscope is installed for this reflectometer in order to increase the spatial resolution (radial observation points).

In this paper, we describe the improved system and its characteristics in section II. Section III presents some plasma experimental data, which is used to demonstrate successful implementation and to validate the cross-diagnostic comparisons of velocity measurements. Finally, in section IV we provide the summary.

II. DIAGNOSTIC DESCRIPTION

A. Microwave frequency comb Doppler reflectometer system

Figure 1 shows the schematic of the current Ka-band microwave frequency comb Doppler reflectometer system. This microwave system is described in detail in Ref 17. The frequency comb source, which is a passive, nonlinear transmission line (PSPL model 7112), can generate an array of equally spaced frequencies, which are controlled by the frequency of the stable synthesized signal generator (SG). The frequency range of the output is initially up to 20 GHz. After the amplified and frequency doubler, Ka-band (26 - 40 GHz) microwave comb is provided. A local oscillator (LO) is used for the heterodyne detection. The

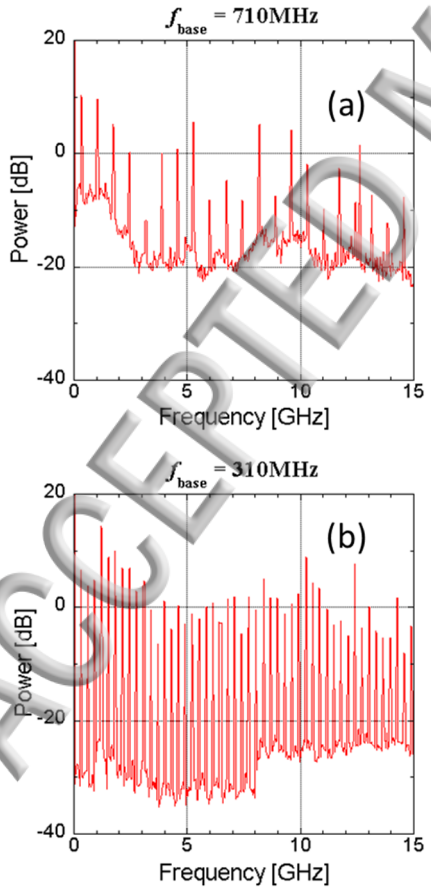

FIG. 2. (Color online). Examples of frequency spectrum of Mixer 1 output (*Signal*) in two cases of base frequency. Base frequency is (a) 710 MHz and (b) 310 MHz.

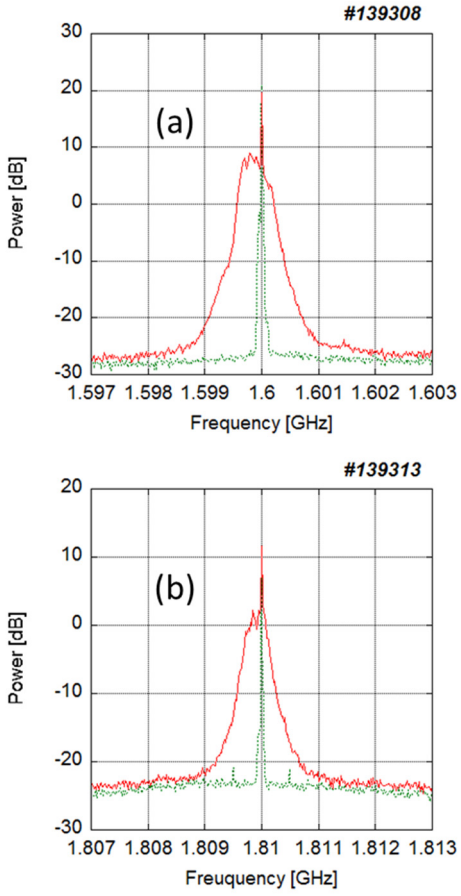

FIG. 3. (Color online). Examples of Doppler shifted frequency spectra around the (carrier) probing microwave frequency of 31 GHz in two different modulation operations. Each base frequency is (a) 710 MHz and (b) 310 MHz. Here, the green dotted lines show the carrier frequency spectra.

power and frequencies of SG and LO can be controlled remotely between the plasma discharges. Two intermediate frequency (IF) components, which are indicated as "*Reference*" and "*Signal*" are generated in each Mixer. In order to estimate the Doppler shifted frequency $f_{Doppler}$ during the whole plasma discharge time, the filter bank system that comprises eight band pass filters is utilized for the in/quadrature (IQ) phase detection. The output of IQ detection signal is led to the analog to digital convertors (ADCs) with the sampling rate of 1 and 10 MHz. Especially, a part of *Signal* is fed to an electro-optical converter set (E/O and O/E, which frequency range is 0.1 - 12 GHz) and transmitted via a 100 m optical fiber directly to the oscilloscope in the diagnostic room. The specifications of the oscilloscope (Teledyne LeCroy model WaveMaster 820Zi-B) are as follows: The sampling rate is 40 G Sample/sec at 4 channel operation, the bandwidth is 20 GHz, and the memory size is 256 M Words/channel. The LABCOM data acquisition system[21-23] collects all of the acquired signal on the real-time and also controls the acquisition setting via their web site.

B. Characteristics of frequency comb signal through a fast digital data acquisition

The number of frequency combs can be controlled by the base SG frequency f_{base}. Figure 2 shows the frequency spectrum of *Signal*. The original designed f_{base} is 710 MHz (we call this *normal* mode operation). The number of combs is around 20 in Ka-band. However, the number of band pass filters in filter bank limits the radial observation points to eight. If we acquire the whole *signal* waveform, the observation points can be increased. Furthermore, in smaller f_{base}, more detailed radial profiles would be obtained. For example, when f_{base} is 310 MHz (*hyper* mode operation), more than 45 comb components are available as shown in Fig. 2(b).

In order to lower the IF frequency, the LO frequency is set to approximately the center frequency of the Ka-band, and it is necessary to pay attention to overlapping IF frequencies especially when changing the operation mode f_{base}. Comparing the characteristics in both modes of operation, the IF frequency and the signal power are found to be different even if they have the same probe frequencies. This is because when the LO frequency is changed, the characteristics of IF amplifier are not flat in the frequency domain. Figure 3 shows the Doppler shifted frequency spectra around the (carrier) probing microwave frequency of 31 GHz in two different operations. In the *normal* mode operation (f_{base} = 710 MHz), the peak amplitude of the scattered signal is more than 35 dB larger than the noise floor. On the other hand, in the *hyper* mode operation (f_{base} = 310 MHz), the amplitude decreases, but it is still more than 23dB larger than the noise floor and the $f_{Doppler}$ can be estimated. Therefore, usually we use the *normal* mode, because the band pass filters are designed for this mode of operation and are out of range in the *hyper* mode of operation.

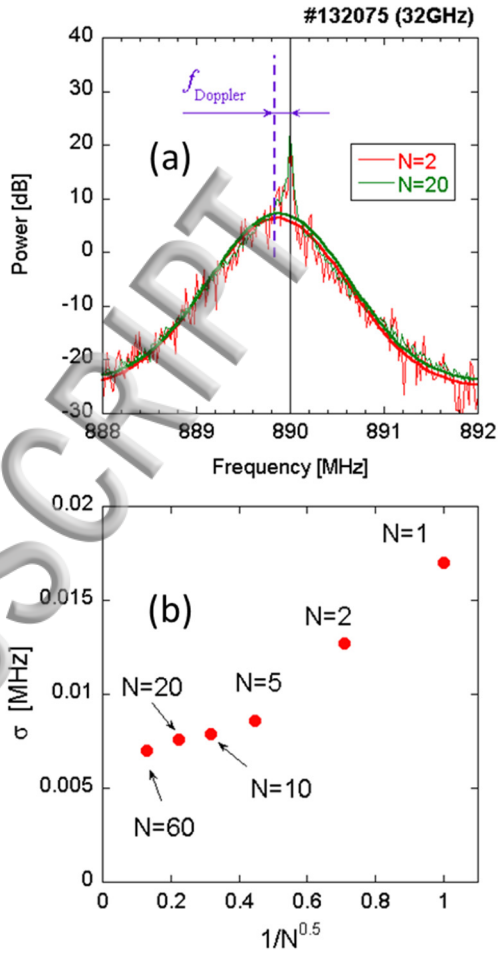

FIG. 4. (Color online). Estimation accuracy of the Doppler shifted frequency. (a) 2 (red) and 20 (green) sample averaging frequency spectra. Here, each thick solid line shows the Gaussian fitting result. (b) The standard error σ as a function of the number of ensemble N.

In general, the ambiguity at the estimation process of $f_{Doppler}$ from the frequency spectra of the scattered wave signal is reduced by the ensemble average. If we use the large number of the ensemble, however, the temporal resolution becomes worse. The frequency spectrum is calculated by the fast Fourier transform (FFT). The number of data samples for one FFT calculation is 4,194,304 (= 2^{22}) in this study. In this case, the frequency resolution of $f_{Doppler}$ estimation is 4.7 kHz. The ambiguity is evaluated by the standard error σ of the Gaussian fitting process. In the LHD plasma experiment, the scattered frequency spectra of 32 GHz probing microwave component are shown in Fig. 4(a). The center frequency (black vertical line) is the carrier frequency of IF signal and has the bandwidth of 0.1 MHz around the center frequency is eliminated in the $f_{Doppler}$ estimation process. The increasing ensemble case (N=20) looks much smoother than the case of N=2. The standard error σ is plotted as a function of the number of the ensemble as shown in Fig. 4(b). It is clear that the increasing number ($N \rightarrow \infty$) leads the unambiguity. In addition, 10 kHz ambiguity means almost 0.1 km/s in velocity measurement.

The range N =10 is selected for the $f_{Doppler}$ estimation in this direct digital data acquisition system. This selection of N =10 is sufficient to reduce the ambiguity and has the temporal resolution of 0.1ms.

III. PLASMA MEASUREMENTS

A. Comparison with filter bank system

The obtained value of $f_{Doppler}$ in the new acquisition system is compared with the estimated value utilized in the conventional filter bank IQ detection system in the LHD plasma discharge. The experiment is carried out under the condition that the magnetic axis position in the vacuum field is R_{ax} = 3.60 m, the magnetic field strength is B_t = 1.375 T, the helical coil pitch parameter γ = 1.2538, and the ratio of the quadrature field B_q = 100 %. The Doppler shifted frequencies $f_{Doppler}$ of 33 GHz are obtained as shown in Fig. 5(c). During the continuous neutral beam injection (NBI) heating, the electron density increases and, after around t = 3.4 s, the cutoff surface appears in the plasma. The IQ detection system can give us the estimated $f_{Doppler}$ value during the whole plasma discharge every 10 μs. On the other hand, because of the limitation of the memory size of the oscilloscope, we apply two types of operation for the data acquisition. One is the batch operation. In this operation, we use whole memory continuously in 6.4 ms and the temporal resolution of the estimated $f_{Doppler}$ is 100 μs. Another case is the burst-like sequence operation. In this operation, total memory is divided into 60 segments during the whole plasma discharge and the data is acquired every 30 ms. The latter operation is used for this comparison. As shown in Fig. 5(c), both estimated $f_{Doppler}$ are in quite good agreement in the stationary plasma.

Another example of dynamic experiment is shown in Fig. 6. In this discharge, the power of perpendicular NBI (p-NBI) is modulated. It is found that the stored energy Wp and the estimated $f_{Doppler}$ also oscillates with NBI modulation period as shown in Fig. 6(b) and (c). Just after the p-NBI injects, the stored energy increases and the estimated $f_{Doppler}$ decreases. In addition, it is known that the flow velocity varies with the modulated tangential NBI[10, 17]. In this time, it is found that the p-NBI can also affect the flow velocity. The estimated $f_{Doppler}$ values are sometimes slightly different in this observation. One of the reasons of this discrepancy might be caused by the sequential data acquisition and the acquired timing may sometimes match the switching time of NBI modulation.

B. Radial profile of $V_\perp$

The Doppler reflectometer is expected to measure the radial profile of perpendicular velocity $v_\perp$. For this aim, the radial observation position and the wavenumber $k_\perp$ is calculated by the ray tracing code LHDGAUSS[24, 25] which uses the radial profile of electron density and temperature measured by Thomson scattering method[26]. Figure 7 shows the radial profile of $v_\perp$ in the *hyper* mode operation as the comb output and batch operation as the data acquisition.

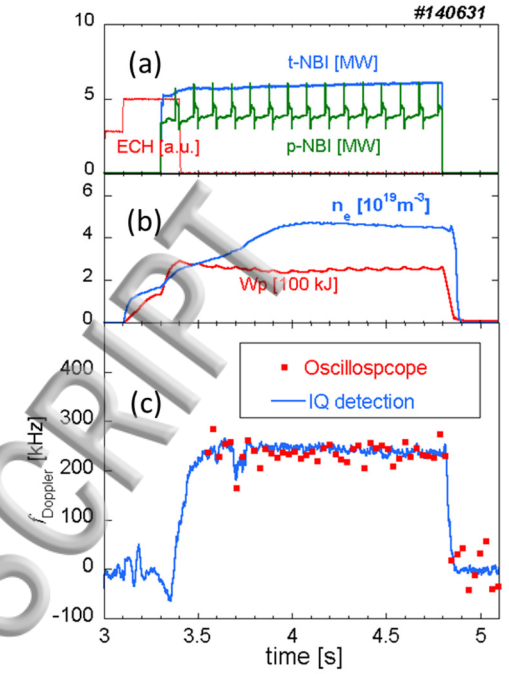

FIG. 5. (Color online). Temporal behavior of (a) the electron cyclotron heating (ECH), tangential neutral NBI (t-NBI), and perpendicular NBI(p-NBI)), (b) the line-averaged electron density n_e and the stored energy Wp, and (c) the Doppler shifted frequency of 33 GHz. Here, blue solid line shows the extraction from the IQ signal using the filter bank system. Red dots show the extraction from the fast oscilloscope acquisition system (trigger time is t = 3.5 s). After t > 4.8 s, the data scattering of the oscilloscope extracted $f_{Doppler}$ is caused by the termination of the plasma.

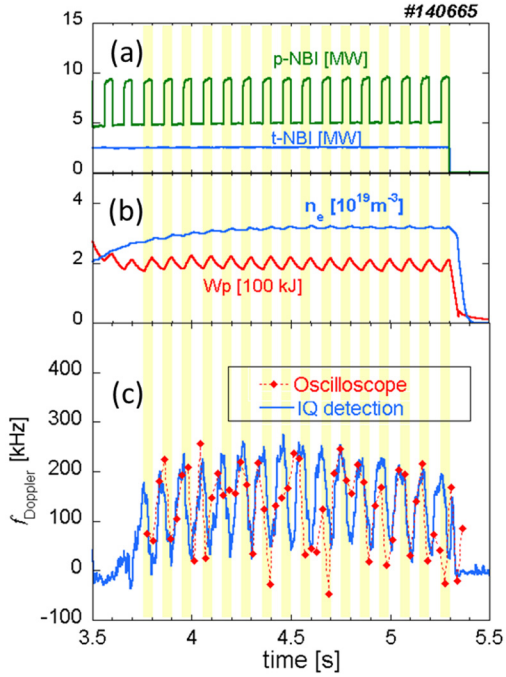

FIG. 6. (Color online). Temporal behavior of (a) continuous tangential t-NBI and modulated perpendicular p-NBI, (b) the line-averaged electron density and the stored energy Wp, and (c) the Doppler shifted frequency of 33 GHz. Blue solid line shows the extraction from the IQ signal using the filter bank system. Red dots show the extraction from the fast oscilloscope direct acquired system (trigger time is t = 3.75 s).

Here, r_{eff} is the effective minor radius and a_{99} is the effective minor radius of which encloses 99% of the total electron pressure[27]. This results are obtained under the experimental condition that R_{ax} = 3.60 m, B_t = 2.75 T, γ = 1.2538, and B_q = 100 %. By heating with the ECH and NBI, the central electron density, electron temperature, and ion temperature is 2.5x10^{19} m^{-3}, 3 keV, and 1.5 keV, respectively. The error bars of DBS data are estimated by the deviation in the 60 time slices between 6.4 ms. The calculated $E \times B$ drift velocity $v_{E\times B}$, which is obtained by the charge exchange spectroscopy (CXS) [28, 29], and plasma pressure profile data, is also plotted. It is found that they are nearly in agreement, that is $v_\perp$ (= $v_{E\times B}$+v_{ph}) ~ $v_{E\times B}$. This result means that v_{ph} is not effectively large rather than $v_{E\times B}$ in the LHD plasma edge region at least at this time. In addition, it can be seen that only a few data points at r_{eff}/a_{99} ~ 1.07 are different. This location is close to the rational surface of $\iota/2\pi$ =2 in vacuum condition and it might be some effect of the magnetic island[30, 31], because both diagnostics are separated in toroidally as shown in Fig. 8 and the phase of magnetic island follows the toroidal location. The future research with MSE measurement is necessary for this understanding. Therefore, the fine $v_\perp$ profile observed by the direct signal acquisition is utilized.

IV. SUMMARY

The fast data acquisition system consisting of the wideband oscilloscope is applied to the microwave frequency comb Doppler reflectometer in LHD. The $f_{Doppler}$ estimation scheme for this system is constructed and the temporal behavior of $f_{Doppler}$ is confirmed to be in agreement with the $f_{Doppler}$ value obtained by the conventional IQ detection system. Also, the fine radial profile of $v_\perp$ is obtained and its result is verified with other diagnostics.

ACKNOWLEDGMENTS

The authors would like to thank the technical staff of LHD for their support of these experiments. The authors also would like to thank Mrs. Y. Tsuji and T. Uto of Teledyne LeCroy Japan Corporation for their support of the fast digital data acquisition system. The present study was supported in part by KAKENHI (Nos. 17K18773, 17H01368, 15H02335, and 15H02336), by a budgetary Grant-in-Aid from the NIFS LHD project under the auspices of the NIFS Collaboration Research Program, and by the Collaborative Research Program of Research Institute for Applied Mechanics, Kyushu University. Additional support was provided by Japan/U.S. Cooperation in Fusion Research and Development.

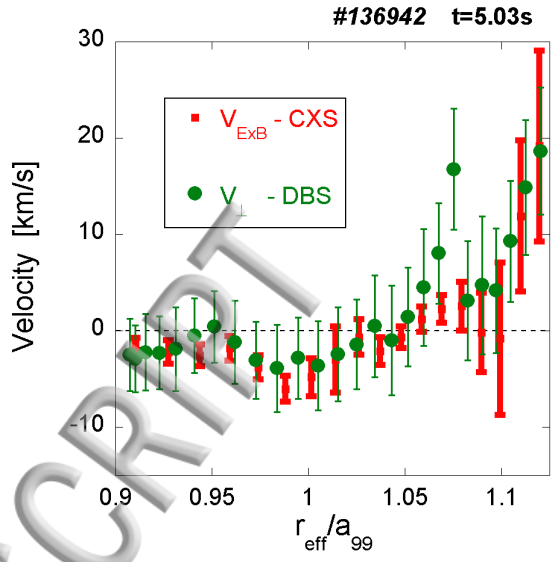

FIG. 7. (Color online). Radial profiles of perpendicular velocity obtained by Doppler reflectometer (green circle) and the E_r x B velocity obtained by CXS (red square).

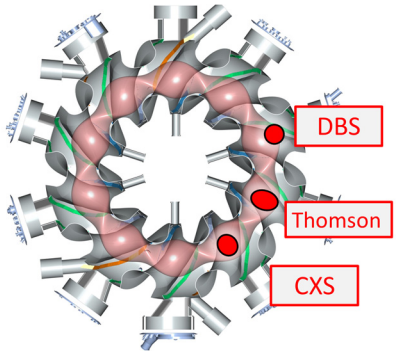

FIG. 8. (Color online). Schematic drawing of toroidal locations of the Doppler reflectometer DBS, the Thomson scattering, and the charge exchange spectroscopy CXS.

[1] T. Tokuzawa, Nuclear Fusion **57**, 025001(2017).
[2] M. Hirsch *et al.*, Plasma Phys. Controlled Fusion **43**, 1641 (2001).
[3] V.V.Bulanin *et al.*, Plasma Phys. Rep. **26**, 813 (2000).
[4] G.D.Conway *et al.*, Plasma Phys. Controlled Fusion **46**, 951 (2004).
[5] J. Schirmer *et al.*, Plasma Phys. Controlled Fusion **49**, 1019 (2007).
[6] P. Hennequin *et al.*, Rev. Sci. Instrum. **75**, 3881 (2004).
[7] P. Hennequin *et al.*, Nucl. Fusion **46**, S771 (2006).
[8] J. C. Hillesheim *et al.*, Rev. Sci. Instrum. **80**, 083507 (2009).
[9] W. A. Peebles *et al.*, Rev Sci Instrum **81**, 10D902 (2010).
[10] J. C. Hillesheim *et al.*, Rev. Sci. Instrum. **80**, 083507 (2009).
[11] N. Oyama *et al.*, Plasma Fusion Res. **6**, 1402014 (2011).
[12] J.C. Hillesheim *et al.*, Nucl. Fusion **55** 073024 (2015).
[13] J.C. Hillesheim *et al.*, Phys. Rev. Lett. **116**, 065002 (2016).
[14] M. Hirsch *et al.*, Rev. Sci. Instrum. **72**, 324 (2001).
[15] T. Happel *et al.*, Rev. Sci. Instrum. **80**, 073502 (2009).
[16] T. Tokuzawa *et al.*, Rev. Sci. Instrum. **83**, 10E322 (2012).
[17] T. Tokuzawa *et al.*, Plasma Fusion Res. **9**, 1402149 (2014).
[18] Y. Takeiri *et al.*, Nucl. Fusion **57**, 102023 (2017).
[19] M. Nunami *et al.* Plasma Phys. Control. Fusion **59**, 044013 (2017).
[20] K. Tanaka *et al.*, Nucl. Fusion **57**, 116005 (2017).
[21] H. Nakanishi *et al.*, IEEE Trans. Nucl. Sci. **63**, 222 (2016).
[22] H. Nakanishi *et al.*, Nucl. Fusion **51**, 113014 (2011).
[23] H. Nakanishi *et al.*, Fusion Sci. Tech. **58**, 445 (2010).
[24] S. Kubo *et al.*, "ECH Power Deposition Study in the Collisonless Plasma of LHD" in Proceedings of 11th Int. Congress on Plasma Physics (July 2002, Sydney, Australia) p.133 (2002).
[25] T. Ii Tsujimura *et al.*, Nucl. Fusion **55**, 123019 (2015).
[26] I. Yamada *et al.*, Fusion Sci. Technol. **58**, 345 (2010).
[27] C. Suzuki *et al.*, Plasma Phys. Control. Fusion **55**, 014016 (2013).
[28] K. Ida *et al.*, Rev. Sci. Instrum. **71**, 2360 (2000).
[29] M. Yoshinuma *et al.*, Fusion Sci. Technol. **58**, 375 (2010).
[30] K. Ida *et al.*, Phys. Rev. Lett. **88**, 015002 (2002).
[31] T. Tokuzawa *et al.*, Nucl. Fusion **57**, 076003 (2017).